ACCEPTED VERSION

Shao-Jian Zhang, Junnan Hao, Han Wu, Qianru Chen, Yiyang Hu, Xun Zhao, and Shi-Zhang Qiao

Coordination Chemistry toward Advanced Zn–I_2 Batteries with Four-Electron $I^-/I^0/I^+$ Conversion

Journal of the American Chemical Society, 2025; 147(19):16350-16361

This document is the Accepted Manuscript version of a Published Work that appeared in final form in Journal of the American Chemical Society, copyright ©2025 American Chemical Society after peer review and technical editing by the publisher. To access the final edited and published work see https://dx.doi.org/10.1021/jacs.5c02085

PERMISSIONS

https://pubs.acs.org/page/authors/sharing.htm#post-accepted

Posting Accepted Manuscripts and Published Articles on Websites and Repositories

Authors may post the Accepted Manuscript or Published Article on personal websites, publicly accessible repositories, or private collaboration groups under these conditions:

- Posting is mandated by an author's funder, institution, or employer.
- If posting is required sooner than 12 months after publication, authors may seek a waiver or choose immediate availability via an Article Development Charge or ACS Open Access option.
- If allowed after 12 months, the Accepted Manuscript may be posted with this notice: *"This document is the Accepted Manuscript version of a Published Article that appeared in final form in [Journal Title], copyright © [insert copyright notice]. To access the final published article, see ACS Articles on Request."*

Posting must be non-commercial and comply with ACS Ethical Guidelines to Publication of Chemical Research. A digital file of the Published Article may only be made publicly available via an ACS Open Access option. Authors may share links to the Published Article on the ACS website using the ACS Articles on Request link.

3 August 2026

http://hdl.handle.net/2440/147282

Coordination Chemistry towards advanced Zn-I_2 batteries with four-electron $I^-/I^0/I^+$ conversion

Shao-Jian Zhang[a], Junnan Hao[a], Han Wu[a], Qianru Chen[a], Yiyang Hu[a], Xun Zhao[a] and Shi-Zhang Qiao[a]*

[a] School of Chemical Engineering, The University of Adelaide, Adelaide, SA 5005, Australia

KEYWORDS: Four-electron iodine conversion, shuttle effect, I^+ hydrolysis, Zn utilization, pouch cell

ABSTRACT: Aqueous zinc-iodine (Zn-I_2) batteries with four-electron (4e) $I^-/I^0/I^+$ conversion (4eZIBs) offer high energy density but face significant challenges for application, including the polyiodide shuttle effect and I^+ hydrolysis for the I_2 cathodes, and poor reversibility for the Zn anodes. Here, we report a coordination chemistry strategy to address these issues simultaneously by introducing hexamethylenetetramine (HMTA) as an electrolyte additive. In aqueous electrolytes, HMTA undergoes protonation to form positively charged nitrogen moieties that effectively precipitate the polyiodides and I^+ species (ICl_2^-) to mitigate the polyiodides shuttle and I^+ hydrolysis. This strategy enables 4eZIBs to achieve a near-theoretical specific capacity of 425 mAh g^{-1} (based on mass of iodine) and a Coulombic efficiency exceeding 99%. On the Zn anode, HMTA preferentially adsorbs onto its surface, inhibiting competitive water adsorption to suppress both Zn dendrite formation and hydrogen evolution. As a result, we achieve durable 4eZIB performance in pouch-cell configurations for the first time. A 0.5 Ah pouch cell with 15% Zn utilization exhibits a high energy density of 113.0 Wh kg^{-1} (based on the mass of cathodes and anodes) and excellent cycling stability over 1,000 cycles, highlighting the potential of 4eZIBs for next-generation energy storage systems.

INTRODUCTION

The growing demand for efficient and sustainable energy storage systems has spurred research into battery technologies beyond conventional lithium-ion batteries.[1, 2] Aqueous zinc-based batteries, which employ Zn metal anodes, present notable advantages such as high safety, low cost, environmental compatibility, and impressive energy/power density.[3-5] Among these, rechargeable aqueous Zn-I_2 batteries (ZIBs) have gained attention as promising candidates due to their fast redox kinetics and multi-electron electrochemistry.[6-9] Traditional ZIBs rely on a two-electron (2e) I^-/I^0 redox reaction (2eZIBs), delivering a redox potential of 0.54 V *vs.* standard hydrogen electrode (SHE) and a theoretical capacity of 211 mAh g_{iodine}^{-1}.[10, 11] However, limited theoretical energy density of 2eZIBs is unsatisfactory compared to the prevailing Zn-MnO_2 systems (308 mAh g^{-1} and 0.57 V *vs.* SHE).[12, 13] Recently, 4eZIBs have emerged as an attractive alternative, leveraging the $I^-/I^0/I^+$ redox pathway to achieve a higher redox potential (1.08 V for I^0/I^+ and 0.54 V for I^-/I^0 *vs.* SHE) and a doubled theoretical capacity of 422 mAh g_{iodine}^{-1}.[12, 14, 15] Despite these advantages, the practical implementation of 4eZIBs faces significant challenges. The polyiodide shuttle effect during the I^-/I^0 conversion and water-induced hydrolysis of I^+ species (*e.g.*, ICl or ICl_2^-) during the I^0/I^+ conversion severely hinder reversibility.[16, 17] To achieve highly reversible 4eZIBs, it is essential to address both the polyiodide shuttle effect and the I^+ hydrolysis simultaneously.

Significant efforts have been devoted to mitigating the shuttle effect in 2eZIBs through strategies such as host material design,[8, 10, 18, 19], functional binders,[20, 21] catalysts,[22-24] ion selective membrane,[25-28] electrolyte engineering,[29-32] and anode protection.[33, 34] However, these approaches generally fall short of enabling highly reversible 4eZIBs, largely due to the persistent challenge of I^+ hydrolysis caused by water's nucleophilic attack.[35] Reducing the water activity of electrolytes is an important approach to mitigating the I^+ hydrolysis, which has been explored by using super-concentrated electrolytes,[14, 36] organic-water hybrid electrolytes,[37] and hydrated eutectic electrolytes.[38] While effective, these approaches increase electrolyte viscosity and cost, thereby compromising battery affordability and reaction kinetics. Recently, quaternary ammonium cations have demonstrated potential in suppressing I^+ hydrolysis within diluted electrolytes through coordination interactions.[17] However, their use raises concerns, as these electrochemically inactive cations often have high molecular weights that can reduce the overall energy density of 4eZIBs. Moreover, the poor Zn reversibility in diluted electrolytes presents additional challenges, including dendrite formation, parasitic hydrogen evolution (HER), and Zn corrosion, all of which severely damage the battery durability.[4, 39, 40] In the pursuit of

practical applications of 4eZIBs, the development of aqueous electrolyte systems that functions to address the issues of shuttle effect and I^+ hydrolysis, together with poor Zn reversibility becomes imperative.

In this work, we address the primary challenges associated with both I_2 cathodes and Zn anodes in 4eZIBs by introducing hexamethylenetetramine (HMTA) as an additive in a diluted electrolyte. In aqueous electrolytes, HMTA undergoes protonation to form positively charged nitrogen moieties (-NH^+), which bind to polyiodides and ICl_2^- anions through ionic interactions. This process effectively suppresses the polyiodide shuttle effect and enhances the stability of I^+ species against hydrolysis. Additionally, HMTA preferentially adsorbs onto the Zn surface, where it competes with water molecules to reduce parasitic HER. Adsorbed HMTA also coordinates with Zn^{2+} ions, facilitating de-solvation and regulating Zn plating/stripping behavior to suppress dendrite formation. As a result, the 2eZIBs achieve a high specific capacity of 215 mAh g_{iodine}^{-1} and high battery CE of exceeding 99% at 0.2 A g^{-1}, along with exceptional durability of nearly 25,000 cycles at 4 A g^{-1}. More importantly, the coordiantion effect of HMTA significantly improves the reversibility of 4eZIBs, enabling a near-theoretical capacity of 425 mAh g_{iodine}^{-1} at 0.4 A g^{-1}, and long-term durability of 5,000 cycles at 4 A g^{-1}. By simultaneously optimizing the performance of both cathodes and anodes, the HMTA additive enables impressive cyclability in pouch-cell configurations for both 2e and 4eZIBs under limited Zn supply. Under the conditions of high-loading cathodes (~18.5 mg_{iodine} cm^{-2}) and high Zn utiliation rate (ZUR, *ca.* 43%), a 0.5 Ah 2e Zn-I_2 pouch cell can deliver a distinguished lifespan of 672 cycles with 80% retentive capacity. Notably, the practical demonstration of 4eZIBs is assessed in pouch-cell configuration for the first time. A 0.5 Ah 4e Zn-I_2 pouch cell operated at a ZUR of 15% achieves a high energy density of 113.0 Wh kg^{-1} (based on the mass of cathodes and anodes) and an outstanding cycling performance of 1,000 cycles with 88.8% retentive capacity.

RESULTS AND DISCUSSION

Coordination effects of HMTA on iodine conversion. HMTA is a cage-like heterocyclic organic compound with the chemical formula $(CH_2)_6N_4$ (**Figure 1**a). The N atoms in HMTA are rich in lone pair electrons, presenting negative electrostatic potential (**Figure S1**). In aqueous media, N atoms readily accept protons to form positively charged moieties (–NH^+), which can strongly bond with polyiodides and ICl_2^-. For this study, 2 M $ZnSO_4$ with 0.5 M NaCl aqueous solution (denoted as ZS/NaCl) was used as base electrolyte, where NaCl serves as a source of Cl^- ions to facilitate the I^0/I^+ conversion. HMTA was introduced into the ZS/NaCl electrolyte as an additive. Due to the alkaline nature of HMTA solutions (**Figure S2**), its concentration in Zn^{2+}-based electrolytes is typically limited to low levels (< 5 mM).[41] However, by adjusting the pH value of electrolytes with H_2SO_4 solution, the solubility of HMTA in ZS/NaCl electrolyte is significantly enhanced, allowing concentrations of up to 1 M (**Figure S3** and **S4**). The ZS/NaCl electrolytes containing varying concentrations of HMTA are designated as ZS/NaCl-*m*HMTA, where *m* represents the HMTA concentration in molarity (M).

The impact of HMTA on mitigating shuttle effects in 2eZIBs was firstly investigated. The –NH^+ moieties of HMTA can interact with polyiodides to generate insoluble HMTA-I_x composites (where x = 3 or 5), as verified by the appearance of a dark-brown precipitate after mixing HMTA with I_3^- aqueous solutions (**Figure 1**a and b). Raman spectra was collected to analyze the anionic composition of the HMTA-I_x composites. As shown in **Figure 1**c, the I_3^- solution exhibits a prominent Raman band at 114 cm^{-1} and a shoulder band at 148 cm^{-1}, which are attributed to the symmetric and antisymmetric vibration of I_3^- anions, respectively.[42] In contrast, the HMTA-I_x composite reveal distinct bands for I_3^- (*ca.* 108 cm^{-1}) and I_5^- (*ca.* 155 cm^{-1}),[8] confirming that HMTA effectively precipitates a variety of polyiodide species.

To evaluate the suppression of shuttle effects by HMTA additives, *in-situ* ultraviolet-visible (UV-vis) spectroscopy was conducted to monitor the dissolution of I_3^- during the 2e conversion by using a home-made quartz battery (**Figure S5**).[30] In ZS/NaCl electrolyte, the absorbance of I_3^- at 285 nm and 350 nm increase steadily during battery charging and discharging, indicating significant I_3^- dissolution (**Figure 1**d).[10] This observation is consistent with the noticeable yellow discoloration of the quartz battery after cycling (inset in **Figure 1**d). Remarkably, the addition of HMTA to the electrolyte substantially suppresses I_3^- dissolution with much weaker I_3^- absorbance (**Figure 1**e). Quantitative comparison of the I_3^- absorbance at ~285 nm shows that the dissolution of I_3^- in ZS/NaCl electrolyte is over six times higher than in the HMTA-containing electrolyte (**Figure 1**f), clearly demonstrating significant suppression of polyiodide dissolution and shuttle by HMTA additive. It should be noted that the batterie using HMTA-I_x composite as cathodes can deliver a specific capacity of *ca.* 125 mAh g^{-1} (based on the mass of HMTA-I_x) and stable cycling, validating the coordination between HMTA and polyiodides affects less on I^-/I^0 conversion (**Figure S6**).

The impact of HMTA on I^0/I^+ conversion was then investigated. The primary cause of the irreversibility of the I^0/I^+ conversion lies in the pronounced hydrolysis of I^+ species. Similar to polyiodides, the –NH^+ moieties of HMTA can bond with ICl_2^-, which forms a light-yellow precipitate (**Figure 1**g and h). The anionic composition of the precipitate was confirmed by Raman spectroscopy. The precipitate exhibits a sharp Raman band at *ca.* 270 cm^{-1},[17] attributed to the I–Cl vibration for the ICl_2^- (**Figure 1**i). This is consistent with the Raman spectrum of ICl_2^- solutions, indicating the formation of HMTA-ICl_2 composite. To investigate the impact of HMTA coordination on suppressing ICl_2^- hydrolysis, the ICl_2^- solution and HMTA-ICl_2 composite were mixed with ZS/NaCl electrolyte. As shown in **Figure 1**j, when mixing the ICl_2^- solution with ZS/NaCl electrolyte, black precipitate forms immediately, which is confirmed as I_2 solid with a Raman band at *ca.* 180 cm^{-1},[14, 43] indicating the severe hydrolysis of ICl_2^-. In sharply contrast, the light-yellow color of the HMTA-ICl_2 composite remains intact even after one-week immersion. The Raman spectrum further confirms the presence of ICl_2^- without any detectable I_2 generation, strongly validating that HMTA coordination effectively inhibits the hydrolysis

of ICl_2^-. Besides, HMTA-ICl_2 composites are electrochemically active for $I^-/I^0/I^+$ conversion, which exhibits a specific capacity of 214.5 mAh g^{-1} (based on the mass of HMTA-ICl_2) and stable cycling performance (**Figure S7**). Moreover, under a potential range of 0.6-1.9 V, the HMTA-I_x composites also enable good reversibility for $I^-/I^0/I^+$ conversion, indicating that HMTA coordination affects less the conversion between various iodine species (**Figure S8**).To further assess the impact of HMTA coordination on the reversibility of 4eZIBs, the ZS/NaCl-*x*HMTA with varying HMTA concentrations was adopted as electrolytes, where KB loaded with 70% I_2 (KB-I_2) is served as cathodes (**Figure 1**k and l). The batteries with ZS/NaCl electrolytes deliver a low discharge capacity of 318 mAh g^{-1} (based on the mass of I_2), highlighting an insufficient I^0/I^+ conversion rate. As the HMTA concentration increases, the I^0/I^+ contribution and reversibility are progressively enhanced, indicating that HMTA coordination facilitates 4e conversion and mitigates parasitic hydrolysis reactions. Notably, when the HMTA concentration reaches 0.2 M or higher, a near-theoretical discharge capacity of *ca.* 425 mAh g^{-1} is delivered. However,

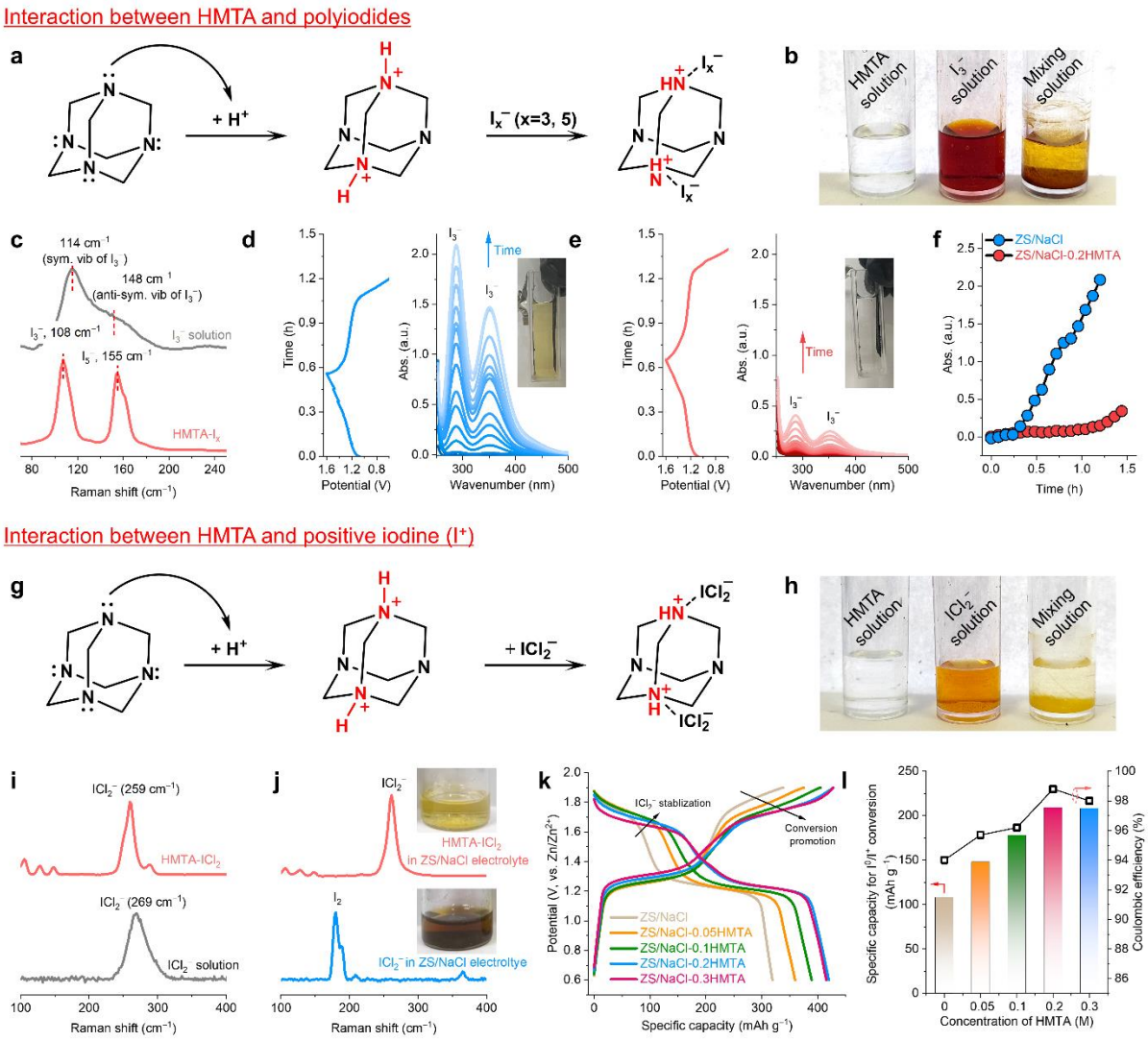


Figure 1. Coordination between HMTA and iodine species. (a) Schematic for the coordination between HMTA and polyiodides. (b) The photographs for the formation of HMTA-I_x precipitate. (c) Raman spectra for the I_3^- solution and HMTA-I_x composite. *In-situ* UV-Vis spectra for the I_3^- dissolution during 2e iodine conversion in (d) ZS/NaCl and (e) ZS/NaCl-0.2HMTA electrolytes. (f) The comparison of the variation of I_3^- absorbance at 285 nm in two electrolytes. (g) Schematic for the coordination between HMTA and ICl_2^- anions. (h) The photographs for the formation of HMTA-ICl_2 precipitate. (i) Raman spectra for the ICl_2^- solution (0.1 M ICl dissolved in 1 M HCl) and HMTA-ICl_2 composite. (j) Raman spectra revealed the hydrolysis of ICl_2^- and HMTA-ICl_2 in ZS/NaCl electrolytes. Insets are the corresponding photographs after resting for one week. (k) The GCD curves of 4eZIBs with different electrolytes at 0.4 A g^{-1}. (l) The I^+ conversion rates and battery CEs with different electrolytes.

higher concentration of HMTA would damage the reversibility of Zn anodes (**Figure S9**). Among them, ZS/NaCl-0.2HMTA was identified as the optimal electrolyte for 4eZIBs, providing excellent $I^-/I^0/I^+$ conversion reversibility and desirable Zn reversibility.

Shuttle-free 2eZIBs by HMTA coordination. The Galvanostatic charge-discharging (GCD) of 2eZIBs were conducted to access the impact of HMTA additive on polyiodide shuttle effect. The KB-I_2 was used as cathodes and the active loading of I_2 is controlled at *ca.* 10 mg_{iodine} cm^{-2}. In ZS/NaCl electrolyte, the initial specific capacity of 2eZIBs is 204.2 mAh g^{-1} at 0.2 A g^{-1} (**Figure 2**a and b). The battery gradually losses its capacity in the following cycles with 85.2% retentive capacity after 210 cycles and suffers from failure thereafter. In contrast, the 2eZIBs using ZS/NaCl-0.2HMTA delivers a higher initial specific capacity of 216.2 mAh g^{-1} and remains 97.2% of its initial capacity after 500 cycles, demonstrating significantly enhanced cycling performance. The CEs of 2eZIBs is a key parameter for assessing the shuttle effect. In ZS/NaCl electrolyte, battery delivers an average CEs of 98.3% within initial 200 cycles (**Figure 2**a). Remarkably, the average CEs of battery can be improved to 99.2% over 500 cycles in ZS/NaCl-0.2HMTA electrolyte, indicating that HMTA effectively suppresses the shuttle effect. Self-discharge, which represents capacity loss during prolonged resting, is another critical factor for the practical application of 2eZIBs.[7] **Figure 2**c shows the self-discharge in two electrolytes after resting at fully charged state. The battery CE of 2eZIBs with ZS/NaCl electrolytes significant decreases to 80.5% after resting for 24 h, corresponding to a self-discharge rate of 19.5%. In contrast, the ZS/NaCl-0.2HMTA electrolyte reduces the self-discharge rate to less than 10% after 24 h. The GCD curves further reveal that the 2eZIBs using ZS/NaCl-0.2HMTA electrolyte encounters smaller voltage drop after resting compared to those with ZS/NaCl electrolyte, verifying the suppressive self-discharge by HMTA additive (**Figure S10**).

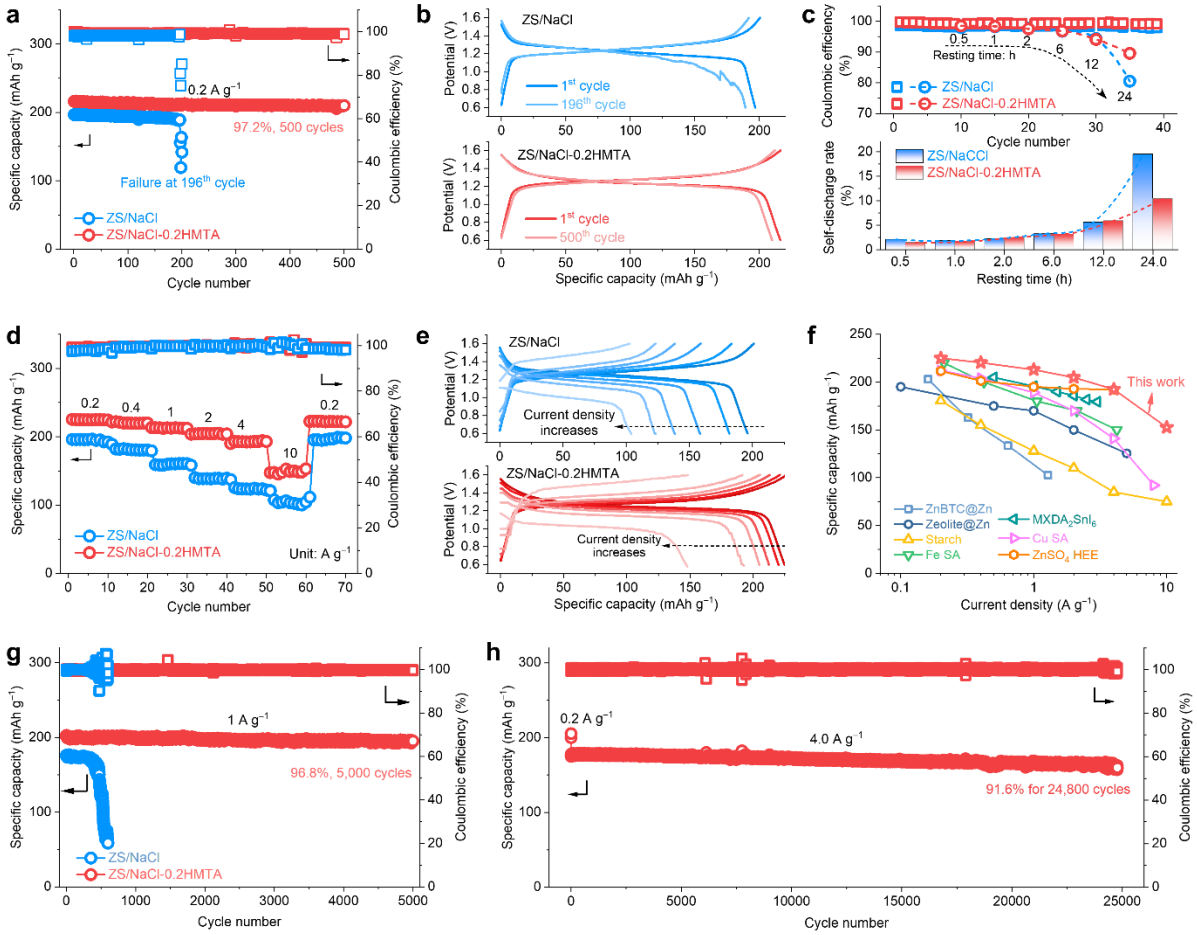


Figure 2. Electrochemical performance of 2eZIBs. (a) The cycling performance and (b) GCD curves of 2eZIBs with ZS/NaCl and ZS/NaCl-0.2HMTA electrolytes at 0.2 A g^{-1}. (c) The battery CEs (top) and self-discharge rate (bottom) after resting of 2eZIBs with ZS/NaCl and ZS/NaCl-0.2HMTA electrolytes. (d) The rate performance and (e) corresponding GCD curves of 2eZIBs with ZS/NaCl and ZS/NaCl-0.2HMTA electrolytes. (f) The comparison of rate performance with reported 2eZIBs. (g) The cycling performance of 2eZIBs with ZS/NaCl and ZS/NaCl-0.2HMTA electrolytes at 1 A g^{-1}. (h) The cycling performance of 2eZIBs with ZS/NaCl-0.2HMTA electrolyte at 4 A g^{-1}.

The rate performance of 2eZIBs was further compared. As shown in **Figures 2**d and 2e, the 2eZIBs using the

ZS/NaCl-0.2HMTA electrolyte demonstrates higher specific capacities and lower battery polarization at all current densities compared to those using the ZS/NaCl electrolyte. Notably, even under an ultra-high current density of 10 A g^{-1} (*ca.* 1 minute for charging), the battery with the ZS/NaCl-0.2HMTA electrolyte achieves a high specific capacity of *ca.* 150 mAh g^{-1}, outperforming the *ca.* 83 mAh g^{-1} capacity with the ZS/NaCl electrolyte. This rate performance significantly surpasses the reported results (**Figure 2**f). The long-term cyclability of 2eZIBs was also investigated. At a current density of 1 A g^{-1}, the battery with the ZS/NaCl-0.2HMTA electrolyte exhibits a high specific capacity of 202.0 mAh g^{-1}, exceeding the 175.7 mAh g^{-1} capacity achieved by ZS/NaCl electrolyte (**Figure 2**g). The 2eZIBs using the ZS/NaCl electrolyte demonstrated stable cycling for only 400 cycles before experiencing rapid degradation. In contrast, the battery with the ZS/NaCl-0.2HMTA electrolyte achieves remarkable stability, maintaining stable cycling over 5,000 cycles with negligible capacity loss (<5%) and minimal polarization increase (**Figures 2**g and **Figure S11**). Even under a high current density of 4 A g^{-1}, the battery with the ZS/NaCl-0.2HMTA electrolyte delivers a high specific capacity of 174.9 mAh g^{-1} and exhibits exceptional durability over 24,800 cycles with a 91.6% capacity retention, highlighting the shuttle-free and long-term performance of 2eZIBs by HMTA coordination (**Figures 2**h and **Figure S12**).

Highly reversible 4eZIBs by HMTA coordination. Although the Cl^- in electrolyte is feasible to activate and stabilize the I^0/I^+ conversion by forming ICl_2^- interhalogen with I^+,[14] the reversibility and conversion rate of I^0/I^+ redox reaction are far from satisfactory due to the hydrolysis of ICl_2^- and sluggish reaction kinetics. As evidence, the CV profile of the 4eZIBs with ZS/NaCl electrolyte presents significant current response from I^-/I^0 redox but much less from I^0/I^+ redox (top of the **Figure 3**a). As demonstrated above, the coordination effect between HMTA and ICl_2^- can promote and stabilize the I^0/I^+ conversion. Thus, in the CV profile of 4eZIBs with ZS/NaCl-0.2HMTA electrolyte, distinct current response for both I^-/I^0 and I^0/I^+ redox is observed (bottom of **Figure 3**a). To investigate the iodine electrochemistry in the ZS/NaCl-0.2HMTA electrolyte, *in-situ* Raman spectra were collected. **Figure 3**b presents the GCD curves for 4eZIBs, and **Figure 3**c exhibits the Raman spectra *in-situ* collected during battery operation. In the region of I^-/I^0 conversion, iodine conversion involves the formation of I_3^- and I_5^- intermediates, which well accords to the previous reports.[8, 22] When the potential is higher than 1.6 V, the Raman band for I_3^- gradually disappears, the Raman band for I_5^- positively move to a higher Raman shift, which is because the polyiodides gradually convert to the I_2. To explicitly observe the conversion between I_2 and I^+, the Raman spectra for I^0/I^+ conversion (spots marked in the **Figure 3**b) were exhibited in **Figure 3**d. When further elevating the charge potential to higher than 1.6 V, the I_2 (180 cm^{-1}) starts to weaken and disappear. Meanwhile, the Raman band for ICl_2^- (260 cm^{-1}) start to emerge and gradually intensify along the charging, indicating the conversion from I_2 to I^+. In the discharging, a reverse trend in iodine conversion is observed, evidencing the reversibility.

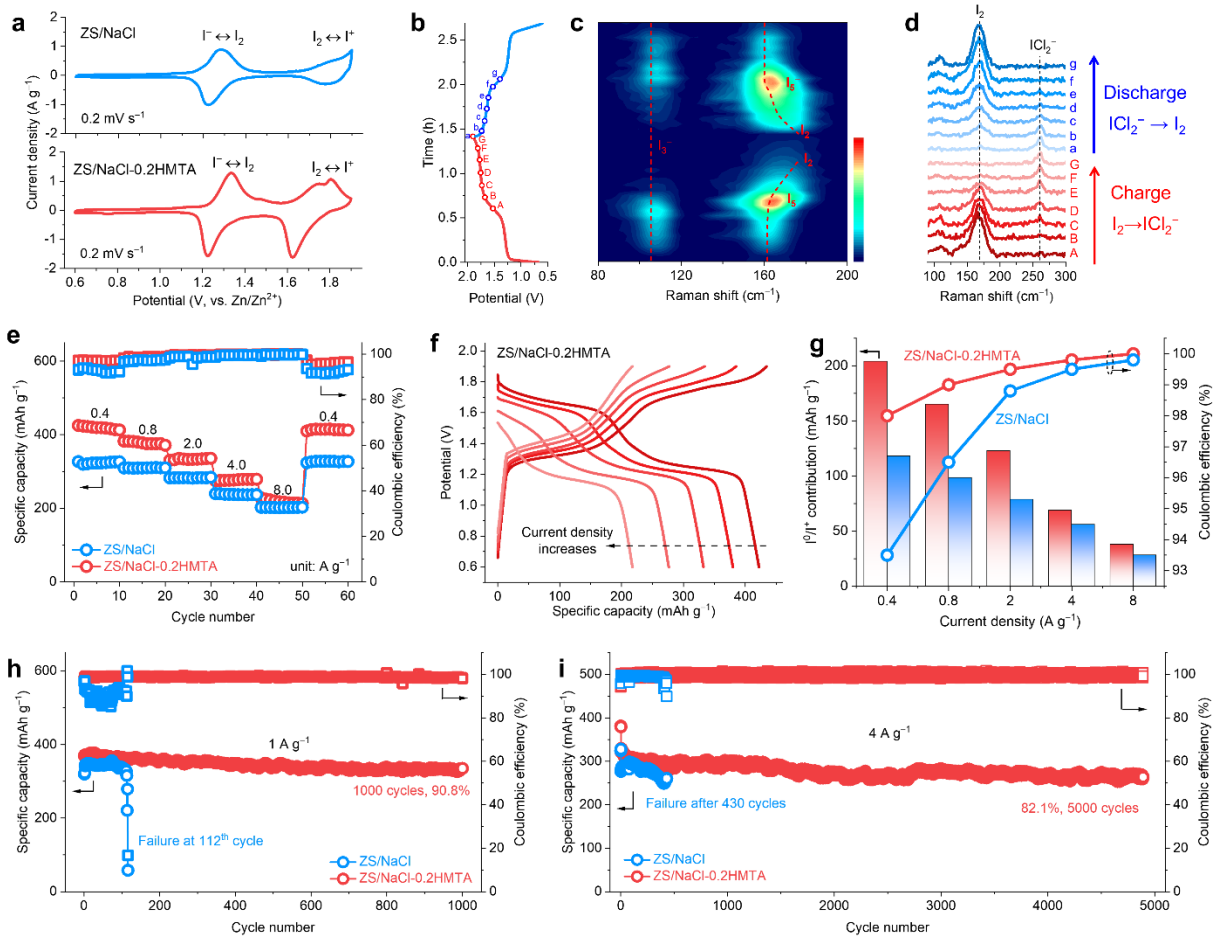


Figure 3. The electrochemical performance of 4eZIBs. (a) The CV profiles of 4eZIBs with ZS/NaCl and ZS/NaCl-0.2HMTA electrolytes. (b) GCD curves and (c) *in-situ* Raman spectra for 4eZIBs with ZS/NaCl-0.2HMTA electrolyte. (d) *In-situ* Raman spectra for the I^0/I^+ region (collection positions are marked in (b)). (e) Rate performance of 4eZIBs with ZS/NaCl and ZS/NaCl-0.2HMTA electrolytes. (f) GCD curves of the 4eZIBs with ZS/NaCl-0.2HMTA electrolyte under different current densities. (g) The comparison of I^0/I^+ contribution and battery CEs of 4eZIBs using two electrolytes under different current densities. Long-term cycling stability of 4eZIBs in two electrolytes at (h) 1 A g^{-1} and (i) 4 A g^{-1}.

The electrochemical performance was investigated to study the impact of HMTA on the reversibility and durability of 4eZIBs. As shown in **Figure 3**e, the 4eZIBs with ZS/NaCl-0.2HMTA electrolyte exhibit a near-theoretical discharge capacity of 424.8 mAh g^{-1} at 0.4 A g^{-1}, surpassing that with ZS/NaCl electrolyte of 338.5 mAh g^{-1}. Corresponding GCD curves further validate that HMTA additive promotes the I^-I^0/I^+ conversion, which presents two flat charge/discharge voltage platforms for I^-/I^0 (~1.35/1.25 V) and I^0/I^+ (~1.76/1.68 V) redox (**Figure 3**f and **Figure S13**). Besides, the 4eZIBs with ZS/NaCl-0.2HMTA electrolyte undergo superior rate capability compared to the counterpart with ZS/NaCl electrolyte, which deliver 424.8, 382.4, 335.1, 278.5, and 215.8 mAh g^{-1} at 0.4, 0.8, 2, 4, and 8 A g^{-1}, respectively (**Figure 3**e). When the current density is reduced back to 0.4 A g^{-1}, the specific capacity can recover to 415.5 mAh g^{-1}, further highlighting the significant reversibility. **Figure 3**g compares the capacity contribution from the I^0/I^+ redox and related battery CEs in two electrolytes. The I^0/I^+ contribution in ZS/NaCl-0.2HMTA electrolyte is around 204 mAh g^{-1} at 0.4 A g^{-1}, which is close to the theoretical value of 211 mAh g^{-1}. While for the 4eZIBs using ZS/NaCl electrolyte, this value is only 118 mAh g^{-1}, suggesting the lower I^0/I^+ conversion rate. At all current densities, the 4eZIBs using ZS/NaCl-0.2HMTA electrolyte all exhibits higher I^0/I^+ contribution and battery CEs, demonstrating the HMTA can promote efficiency and reversibility of I^0/I^+ conversion.

The long-term durability of 4eZIBs in two electrolytes was investigated. As shown in **Figure 3**h and **Figure S14**, owing to the severe ICl_2^- hydrolysis and inferior reaction kinetics, the 4eZIBs with ZS/NaCl electrolyte exhibits low discharge capacity and battery CEs of 323.1 mAh g^{-1} and < 95%, respectively, at 1 A g^{-1}. Battery failure occurs only after 112 cycles, demonstrating the inferior cycling stability. In sharp contrast, with the HMTA additive, the specific discharge capacity of 4eZIBs is enhanced to 371.6 mAh g^{-1} at 1 A g^{-1} and the cycling stability is extended to over 1,000 cycles with 90.8% retentive capacity. Importantly, the CEs of the battery using ZS/NaCl-0.2HMTA are stabilized at over 99%, indicating less I^+ hydrolysis. Subsequently, the cycling performance of 4eZIBs under higher current density was studied (**Figure 3**i and **Figure S15**). In ZS/NaCl electrolyte, the

4eZIBs exhibits poor reversibility and suffers from battery failure after just 430 cycles at 4 A g^{-1}. Significantly, the 4eZIBs in ZS/NaCl-0.2HMTA electrolyte delivers an initial capacity of 321.7 mAh g^{-1} with characteristic 4e voltage profiles. Moreover, battery can sustain over 5,000 cycles with a capacity retention of 82.1%, strongly highlighting the excellent durability of 4eZIBs by the HMTA additive.

High-reversible and dendrite-free Zn anodes by HMAT coordination. As a practical battery, it relies on high-reversible cathodes and anodes simultaneously, therefore the impact of HMTA additive on Zn reversibility was investigated. It was demonstrated that HMTA can tune the Zn^{2+} solvation structure by the coordination between Zn^{2+} ions and HMTA.[41] However, the fact is that the concentration of HMTA in electrolytes is relatively low, implying that the limited impact of HMTA on the bulk solvation structure. Instead, additives are more possible to modulate the Zn/electrolyte interface. To investigate the interfacial behaviour of HMTA on Zn anodes, the Molecular dynamic (MD) simulation showing the dynamic evolution of HMTA on Zn interface was conducted (**Video S1**). Results indicate that HMTA molecules can spontaneously enrich at the Zn interface (**Figure 4**a and b), indicating the preferential adsorption of HMTA at Zn interface. This result well accords to the stronger adsorption of HMTA molecules at Zn (002) facet compared to the free H_2O molecules (**Figure S16**). This strong interfacial interaction would contribute to less HER by repelling the competitive water adsorption.[44]

To study the impact of HMTA adsorption at Zn interface on the parasitic HER, the linear sweep voltammetry (LSV) of the electrolytes was conducted (**Figure S17**). Significant negatively shift of the one-set potentials for the HER and Zn plating demonstrate the suppressive HER by the HMTA. Despite HMTA additive will slightly compromises the OER of electrolytes, it would not affect the stable cycling of 4eZIBs since the upper limits for $I^-/I^0/I^+$ conversion is still far away from the OER. The HER and Zn plating often occurs simultaneously, leading to the failure of precisely detect the parasitic HER during Zn plating.[33] To solve this problem, differential electrochemical mass spectrometry (DEMS) was applied to real-time monitor the on-set potentials for parasitic HER and Zn plating separately. The *in-situ* cell for DEMS measurement is shown in **Figure S18**. The gold (Au) is coated onto the porous polytetrafluoroethylene (PTFE) film *via* magnetron sputtering, which is served as the working electrode. This Au-PTFE film allows the gas to pass through but avoid the leakage of liquid electrolytes. The generated H_2 during Zn plating can be real-time collected by the vacuum chamber below the Au-PTFE working electrode and then analyzed by mass spectrometer. As shown in **Figure 4**c, in ZS/NaCl electrolyte, the current response of HER and Zn plating in LSV curves starts from -0.96 V *vs*. Ag/AgCl, and the H_2 signal in the mass spectrometer emerges from -1.0 V *vs.* Ag/AgCl and significantly intensifies thereafter, suggesting the HER and Zn plating occur simultaneously. In contrast, in the ZS/NaCl-0.2HMTA electrolyte, the current response in LSV curve negatively shifts to -1.0 V *vs.* Ag/AgCl, however the H_2 signal does not appear until the potential reaches to -1.1 V and remains at rather low intensity afterwards, validating HMTA significantly alleviates the parasitic HER.

The interfacial water structure affects largely on the HER activity. Typically, the broad peak located at a wavenumber range of 3000-3600 cm^{-1} is associated to the O–H vibration (**Figure 4**d). The O–H vibration is generally divided into five types of local hydrogen bonds (H-bonds) by a proton donor (D)-acceptor (A) mechanism, that are free-OH (3650 cm^{-1}), DDA-OH (3500 cm^{-1}), DA-OH (3400 cm^{-1}), DDAA-OH (3200 cm^{-1}), and DAA-OH (3050 cm^{-1}).[45] In which, H-bonds of free-OH, DDA-OH, and DA-OH are generally regarded as the weak H-bonds (W-H), whilst that of DDAA-OH and DAA-OH are determined as strong H-bonds (S-H). In aqueous electrolyte for AZBs, the strong Zn^{2+}-H_2O coordination disrupts the tetrahedral structure between H_2O, resulting in the proportion of S-H decreasing and that of W-H increasing.[46] During Zn plating, Zn^{2+}-H_2O coordination presents strong tendency to be reduced to generate H_2.[47] In other words, an interfacial water structure with less Zn^{2+}-H_2O coordination or less W-H network would contribute to less HER. HMTA molecules present stronger binding energy with Zn^{2+} ions compared to the H_2O molecules (**Figure S19**), implying the adsorbed HMTA at the Zn interface can reduce the Zn^{2+}-H_2O coordination, thereby benefiting to suppress the HER.

To probe the impact of HMTA additive on interfacial water structure, the *in-situ* attenuated total reflectance Fourier transform infrared spectroscopy (ATR-FTIR) was conducted during Zn plating process (**Figure 4**e). During the test, the germanium (Ge) prism was used as working electrodes for Zn plating, and Zn foil was used as the counter and reference electrodes (**Figure**

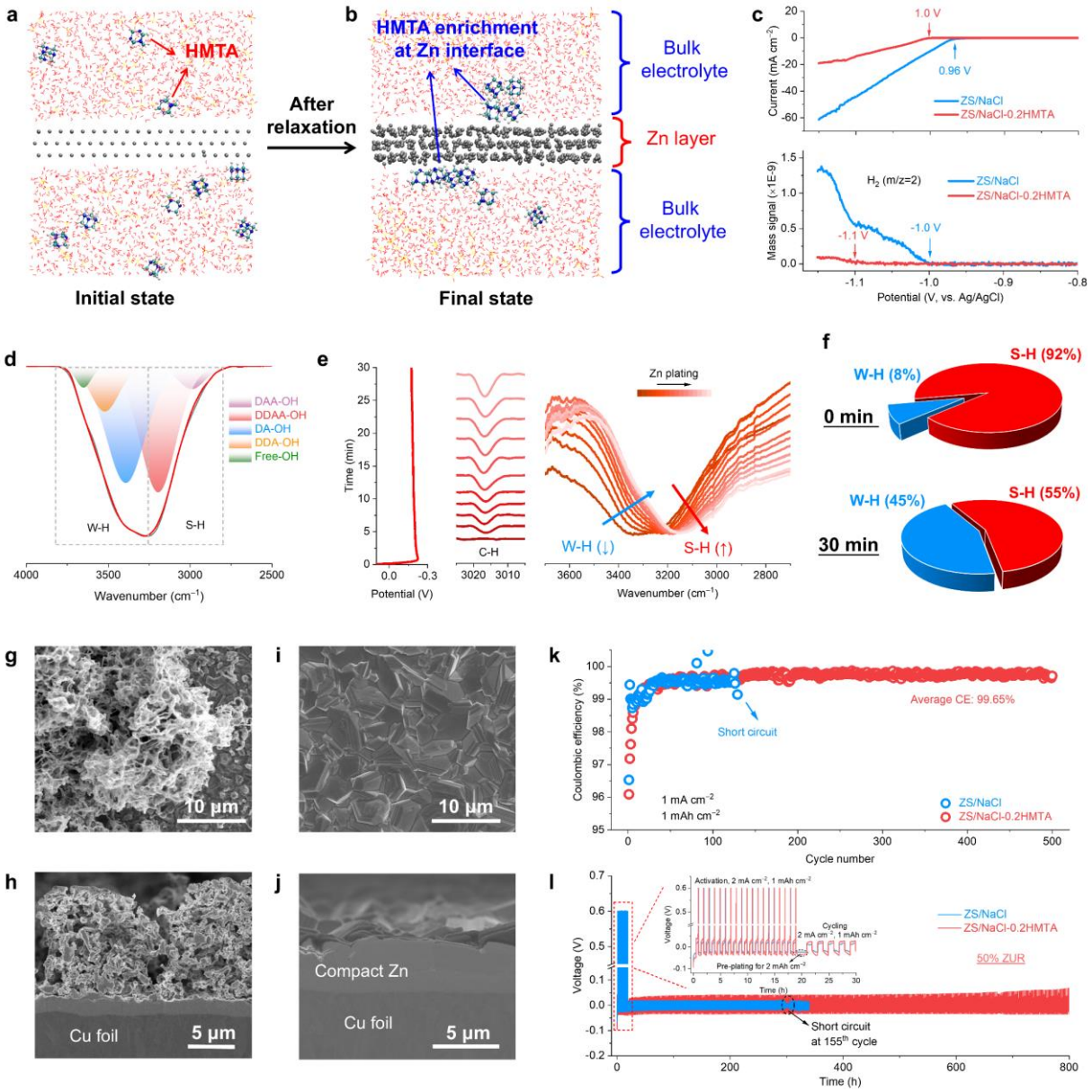


Figure 4. Zn reversibility improvement by HMTA additive. MD simulation for (a) the initial state and (b) final state of HMTA behavior at the Zn interface. (c) LSV curves (top) and corresponding mass signal of H_2 (bottom) for Zn plating. (d) FTIR spectra for the typical water structure. (e) *In-situ* ATR-FTIR for the evolution of interfacial water structure during Zn plating in ZS/NaCl-0.2HMTA electrolyte. Left figure shows the GCD curves for Zn plating, the middle figure is the evolution of C-H vibration during Zn plating, and right figure is the evolution of O-H vibration during Zn plating. (f) The pie charts for the proportion of interfacial W-H and S-H at initial plating (bottom) and after 30 min Zn plating (top). The morphology of (g) surface and (h) cross section of plated Zn in the ZS/NaCl electrolyte. The morphology of (i) surface and (j) cross section of plated Zn in the ZS/NaCl-0.2HMTA electrolyte. (k) The Zn plating/stripping CEs at 1 mA cm^{-2} and 1 mAh cm^{-2}. (l) The Zn plating/stripping stability under conditions of 50% ZUR. Inset is enlarged figure for selected region.

S20). Any variation at the interface during Zn plating can be collected from the Ge prism. During the Zn plating, the C–H vibration (*ca.* 3015 cm^{-1}) gradually intensifies with the Zn plating,[30] suggesting the enrichment of HMTA at Zn interface (middle of **Figure 4**e). Meanwhile, the O–H vibration exhibits a gradual red shift during Zn plating, proving the decreasing of interfacial W-H (right of **Figure 4**e). The proportion of W-H is around 45% in the beginning, while gradually decreases to 8% after 30 min Zn plating (**Figure 4**f). These results clearly elucidate that the HMTA is significantly enriched at Zn interface, which creates a less W-H network at Zn interface, therefore exhibiting significant suppression of parasitic HER.

Subsequently, the Zn plating morphology at a current density of 2 mA cm^{-2} for 1 h was studied by scanning electron microscope (SEM). As shown in **Figure 4**d, the uneven Zn plating morphology in ZS/NaCl electrolyte is observed. Porous Zn layers with obvious protrusion can be found in

the cross section of plated Zn, confirming the severe dendrite growth (**Figure 4**e). In sharp contrast, a dendrite-free Zn morphology constituted by the close-packed Zn hexagonal plates was observed in the ZS/NaCl-0.2HMTA electrolyte (**Figure 4**f). From the cross section, it can be observed that the plated Zn layer is compact and uniform without porous microstructure, validating the HMTA significantly regulates the Zn plating and avoids the Zn dendrite formation (**Figure 4**g).

The suppressive HER and Zn dendrite deservedly contributes to the enhanced Zn reversibility, which is confirmed by the Zn plating/stripping CEs in Zn-Cu half cells. The Zn-Cu half cells with ZS/NaCl electrolyte achieve a Zn plating/stripping CE of ca. 99.0% after 10 cycles, however, suffer from short circuit after 126 cycles, indicating the severe dendrite formation (**Figure 4**h and **Figure S21**a). Significantly, in the ZS/NaCl-0.2HMTA electrolyte, the Zn-Cu half cells present stable cyclability of 500 cycles with a high average CE of 99.65% (**Figure 4**h and **Figure S21**b). Furthermore, under higher current density (5 mA cm^{-2}) and larger cycled Zn capacity (2 mAh cm^{-2}), the Zn-Cu half cells using ZS/NaCl-0.2HMTA can deliver a stable Zn plating/stripping for 450 cycles with a high average CEs of 99.75% and negligible polarization increases, proving the significant Zn reversibility improvement (**Figure S22**). The Zn plating/stripping stability then was studied by the Zn symmetric cells. As shown in **Figure S23**, the Zn symmetric cells using ZS/NaCl electrolyte presents inferior Zn plating/stripping stability at 2 mA cm^{-2} and 1 mAh cm^{-2}, which suffers from short circuit after 80 cycles (80 h). Significantly, the ZS/NaCl-0.2HMTA electrolyte extends the stable Zn plating/stripping to over 600 cycles (600 h), demonstrating the stable Zn/electrolyte interface and suppressive dendrite formation. The X-ray diffraction (XRD) patterns further reveal that the massive parasitic products generate on the Zn anodes after 100 cycles in the ZS/NaCl electrolyte whilst are significantly suppressed in the ZS/NaCl-0.2HMTA electrolyte (**Figure S24**).

In pursuit of high energy density, the limited Zn supplement is essential. Therefore, the stability of Zn plating/stripping under condition of high Zn utilization rate (ZUR) was studied by Zn-Cu half cells. The Cu electrodes were activated for 10 times and then were pre-plated Zn metal with a capacity of 2 mAh cm^{-2}. And then, the Zn-Cu half cells was cycled under conditions of a fixed Zn capacity of 1 mAh cm^{-2} and a current density of 2 mA cm^{-2} (inset in **Figure 4i**). As half of pre-plated Zn participating the following Zn plating/stripping, the voltage profiles of Zu-Cu half cells can reflect the cycling stability under a ZUR of 50%. Owing to the limited Zn supplement from the Cu electrodes, the Zn-Cu half cells present inferior lifespan when using ZS/NaCl electrolyte, reflecting poor Zn reversibility and serious dendrite growth (**Figure 4**i). It can be observed that the Zn on the Cu electrodes is severely consumed after 100 cycles when using ZS/NaCl electrolyte, confirming the inferior Zn reversibility (**Figure S25**a). In contrast, the HMTA additive improves prominently on the lifespan of Zn anodes owing to the suppressive Zn dendrite and parasitic reactions, which can perform stable cycling for around 800 cycles without battery failure (**Figure 4**i). After 100 cycles, a compact Zn layer has well remained (**Figure S25**b), indicating the potential of HMTA additive for realizing practical ZIBs under limited Zn supplement.

Practical demonstration of ZIBs in pouch-cell configuration. To assess the practical application of ZIBs, the pouch cells with high loading I_2 cathodes and limited supplementary Zn anodes were fabricated. Leveraging from the coordination effects of HMTA with various iodine species and Zn anodes, the issues of polyiodides shuttle effects and I^+ hydrolysis for the I_2 cathodes and poor reversibility for the Zn anodes are concurrently addressed. It is widely recognized that the conditions of high active mass loading for the cathodes and high Zn utilization rate (ZUR) for the anodes impact largely on the energy density of batteries, which can provide objective assessment on the energy density and durability of batteries.[12] Therefore, the Zn-I_2 pouch cells with 2e I^-/I^0 conversion and 4e $I^-/I^0/I^+$ conversion was conducted, as shown in **Figure 5**a. To control the ZUR, the Zn pre-plated Cu (Zn@Cu) anodes are served as the anodes, which are fabricated by electrochemically plating Zn metal on Cu substrates with designed Zn capacity by a home-made electroplating bath (**Figure S26** and **S27**).

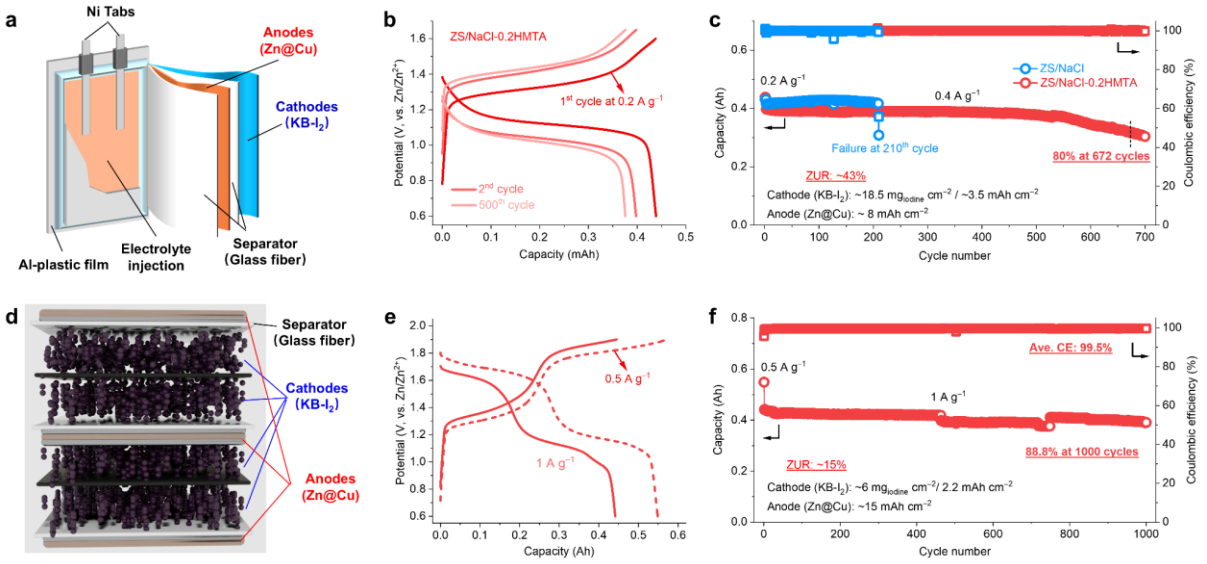


Figure 5. Electrochemical perfroamcne of pouch cells. (a) Schematic for the pouch cell. (b) The GCD curves and (c) cycling performance of 2e Zn-I_2 pouch cell with a ZUR of 43%. (d) The schematic for the internal structure of the muti-layer 4e Zn-I_2 pouch cell. (e) The GCD curves and (f) cycling performance of 4e Zn-I_2 pouch cell with a ZUR of 15%.

The cycling performance of Zn-I_2 pouch cells with 2e I^-/I^0 conversion was studied. In which, a high-loading cathodes (double-side coating, ~18.5 mg_{iodine} cm^{-2} and ~3 mAh cm^{-2} per side) and two Zn@Cu anodes (single-side pre-plated Zn@Cu anodes with a Zn capacity of ~7 mAh cm^{-2}) are matched to assemble the pouch cells. Therefore, the ZUR for this 2e Zn-I_2 pouch cell is controlled at *ca.* 43%. As shown in **Figure 5**b, the Zn-I_2 pouch cell using ZS/NaCl-0.2HMTA electrolyte delivers an initial capacity of 0.44 Ah at 0.2 A g^{-1}. When increasing the current density to 0.4 A g^{-1}, the capacity remains at 0.4 Ah. This pouch cell can store an energy density of 106.2 Wh kg^{-1}, based on the mass of KB-I_2 and Zn metal. Owing to the good reversibility for both I_2 cathode and Zn anodes by the HMTA additive, the Zn-I_2 pouch cell can deliver stable cycling with negligible fading for over 500 cycles and remain 80% of initial capacity after 672 cycles (**Figure 5**b and c). In contrast, the pouch cell using ZS/NaCl electrolyte suffers from battery failure only after 210 cycles (**Figure 5**c and **Figure S28**), suggesting the poor reversibility for both I_2 cathodes and Zn anodes.

Owing to the inferior reversibility for 4e $I^-/I^0/I^+$ conversion, the practical potential for the 4eZIBs is lack of demonstration, especially under pouch cell level. Leveraging from the significant optimization of the reversibility of 4e $I^-/I^0/I^+$ conversion and Zn anodes by HMTA additive, a 4e Zn-I_2 pouch cell with a total capacity of 0.55 Ah was fabricated by sandwiching two I_2 cathodes (double-side coating) and three Zn@Cu anodes (two single-side pre-plated Zn and one double-side pre-plated Zn) (**Figure 5**d). The area capacity for I_2 cathode and Zn anodes is *ca.* 2.2 mAh cm^{-2} (*ca.* 6 mg_{iodine} cm^{-2}) and *ca.* 15 mAh cm^{-2}, respectively, corresponding to a ZUR of *ca.* 15%. As shown in **Figure 5**e, the 4e Zn-I_2 pouch cell exhibits an initial capacity of 0.55 Ah at 0.5 A g^{-1} with two distinguished voltage plateaus, supporting the successful realization reversible 4eZIBs in pouch-cell configuration. Importantly, based on the mass of KB-I_2 cathodes and Zn metal, this pouch cell exhibits an energy density of 113.0 Wh kg^{-1}. When current density increases to 1 A g^{-1}, the capacity is stabilized at 0.44 Ah. Impressively, this pouch cell can withstand ultra-long durability for 1,000 cycles with an 88.8% retentive capacity, proving the excellent reversibility for 4e $I^-/I^0/I^+$ by the HMTA additive (**Figure 5**f and **Figure S29**). By comparing with reported pouch cells for the AZBs, we achieved a remarkable long-durable Zn-I_2 pouch cells with 2e and 4e conversion chemistry, supporting the ZIBs, especially the 4eZIBs, are a promising candidature for large-scale energy storage (**Table S1**).

CONCLUSIONS

In summary, HMTA is used as electrolyte additive to achieve highly reversible 4e $I^-/I^0/I^+$ electrochemistry and Zn plating/stripping stability. On the cathodes, the HMTA is protonated in aqueous electrolytes to generate N^+ centers, which coordinates with polyiodides and I^+ species to prevent the shuttle effect and hydrolysis, respectively. On the Zn anode, xxxxxx. Therefore, the 4eZIBs exhibits a near-theoretical specific capacity of 425 mAh g_{iodine}^{-1} and long-term stability of 5,000 cycles. Besides, *In-situ* FTIR and MD simulation uncover that the HMTA molecules preferentially adsorb at the Zn surface over the water molecules, which reconstruct the interfacial water environment with Zn^{2+}-H_2O coordination, thereby enhancing the Zn reversibility that free of dendrites and HER. Based on this concurrent optimization for both electrodes, 4e Zn-I_2 pouch cells with high cathode loading and controlled ZUR deliver outstanding cyclability. A 0.5 Ah 4e Zn-I_2 pouch cell with a ZUR of 15% was fabricated with a high energy density of 113.0 Wh kg^{-1}, based on the mass of cathodes and anodes. Despite this, the cycling life can be extended to 1,000 cycles with 88.8% retentive capacity. This finding provided strong evidence for the practical adoption of ZIBs with attractive 4e electrochemistry, which is beneficial for developing advanced AZBs for large-scale energy storage.

ASSOCIATED CONTENT

Supporting Information.
This material is available free of charge via the Internet at http://pubs.acs.org.

- MD simulation of the preferential adsorption of HMTA at the Zn interface (MP4)
- Discussion of chemicals, synthesis details, characterizations, electrochemical measurements, SEM, XRD, *in-situ* UV-vis measurement, DEMS, *in-situ* ATR-FTIR measurement, table for the comparison of reported pouch cells.

AUTHOR INFORMATION

Corresponding Author

*Shi-Zhang Qiao
School of Chemical Engineering, The University of Adelaide, Adelaide, SA 5005, Australia;
https://orcid.org/0000-0002-4568-8422;
E-mail: s.qiao@adelaide.edu.au

Authors

Shao-Jian Zhang
School of Chemical Engineering, The University of Adelaide, Adelaide, SA 5005, Australia;
https://orcid.org/0000-0001-7738-0425
Junnan Hao
School of Chemical Engineering, The University of Adelaide, Adelaide, SA 5005, Australia;
https://orcid.org/0000-0002-5777-7844
Han Wu
School of Chemical Engineering, The University of Adelaide, Adelaide, SA 5005, Australia;
https://orcid.org/0000-0002-5281-7325
Qianru Chen
School of Chemical Engineering, The University of Adelaide, Adelaide, SA 5005, Australia;
https://orcid.org/0000-0001-6559-3888
Yiyang Hu
School of Chemical Engineering, The University of Adelaide, Adelaide, SA 5005, Australia;
Xun Zhao
School of Chemical Engineering, The University of Adelaide, Adelaide, SA 5005, Australia;
https://orcid.org/0000-0002-3711-4568

Author Contributions

The manuscript was written through contributions of all authors. All authors have given approval to the final version of the manuscript.

Funding Sources

This work was financially supported by the Australian Research Council (ARC) through Discovery and Linkage projects (FL170100154, DP220102596, LP210301397, and DE230100471).

Notes

The authors declare no competing financial interest.

ACKNOWLEDGMENT

DFT computations were undertaken with the assistance of resources and services from the National Computational Infrastructure (NCI) and Phoenix High Performance Computing, which are supported by the Australian Government and the University of Adelaide.

REFERENCES

(1) Chu, S.; Majumdar, A. Opportunities and Challenges for a Sustainable Energy Future. *Nature* **2012**, *488*, 294-303.
(2) Dunn, B.; Kamath, H.; Tarascon, J. M. Electrical Energy Storage for the Grid: A Battery of Choices. *Science* **2011**, *334*, 928–935.
(3) D. Chao; W. Zhou; F. Xie; C. Ye; H. Li; M. Jaroniec; Qiao., S.-Z. Roadmap for Advanced Aqueous Batteries: From Design of Materials to Applications. *Sci. Adv.* **2020**, *6*, eaba4098.
(4) Yuan, L.; Hao, J.; Kao, C.-C.; Wu, C.; Liu, H.-K.; Dou, S.-X.; Qiao, S.-Z. Regulation Methods for the Zn/Electrolyte Interphase and the Effectiveness Evaluation in Aqueous Zn-Ion Batteries. *Energy Environ. Sci.* **2021**, *14*, 5669-5689.
(5) Kundu, D.; Hosseini Vajargah, S.; Wan, L.; Adams, B.; Prendergast, D.; Nazar, L. F. Aqueous vs. Nonaqueous Zn-ion Batteries: Consequences of the Desolvation Penalty at the Interface. *Energy Environ. Sci.* **2018**, *11*, 881-892.
(6) Li, B.; Nie, Z.; Vijayakumar, M.; Li, G.; Liu, J.; Sprenkle, V.; Wang, W. Ambipolar Zinc-Polyiodide Electrolyte for a High-Energy Density Aqueous Redox Flow Battery. *Nat. Commun.* **2015**, *6*, 6303.
(7) Hao, J.; Zhang, S.; Wu, H.; Yuan, L.; Davey, K.; Qiao, S. Z. Advanced Cathodes for Aqueous Zn Batteries Beyond Zn^{2+} Intercalation. *Chem. Soc. Rev.* **2024**, *53*, 4312-4332.
(8) Zhang, S. J.; Hao, J.; Li, H.; Zhang, P. F.; Yin, Z. W.; Li, Y. Y.; Zhang, B.; Lin, Z.; Qiao, S. Z. Polyiodide Confinement by Starch Enables Shuttle-Free Zn-Iodine Batteries. *Adv. Mater.* **2022**, *34*, 2201716.
(9) Yan, L.; Zhang, S.; Kang, Q.; Meng, X.; Li, Z.; Liu, T.; Ma, T.; Lin, Z. Iodine Conversion Chemistry in Aqueous Batteries: Challenges, Strategies, and Perspectives. *Energy Storage Mater.* **2023**, *54*, 339-365.
(10) Ma, L.; Ying, Y.; Chen, S.; Huang, Z.; Li, X.; Huang, H.; Zhi, C. Electrocatalytic Iodine Reduction Reaction Enabled by Aqueous Zinc-Iodine Battery with Improved Power and Energy Densities. *Angew. Chem. Int. Ed.* **2021**, *60*, 3791-3798.
(11) Li, X.; Li, M.; Huang, Z.; Liang, G.; Chen, Z.; Yang, Q.; Huang, Q.; Zhi, C. Activating the I^0/I^+ Redox Couple in An Aqueous I_2–Zn Battery to Achieve A High Voltage Plateau. *Energy Environ. Sci.* **2021**, *14*, 407-413.
(12) Zhang, S. J.; Hao, J.; Wu, H.; Kao, C. C.; Chen, Q.; Ye, C.; Qiao, S. Z. Toward High-Energy-Density Aqueous Zinc-Iodine Batteries: Multielectron Pathways. *ACS Nano* **2024**, *18*, 28557-28574.
(13) Li, X.; Wang, S.; Zhang, D.; Li, P.; Chen, Z.; Chen, A.; Huang, Z.; Liang, G.; Rogach, A. L.; Zhi, C. Perovskite Cathodes for Aqueous and Organic Iodine Batteries

Operating Under One and Two Electrons Redox Modes. *Adv. Mater.* **2024**, *36*, 2304557.
(14) Zou, Y.; Liu, T.; Du, Q.; Li, Y.; Yi, H.; Zhou, X.; Li, Z.; Gao, L.; Zhang, L.; Liang, X. A Four-Electron Zn-I_2 Aqueous Battery Enabled by Reversible $I^-/I_2/I^+$ Conversion. *Nat. Commun.* **2021**, *12*, 170.
(15) Lin, D.; Li, Y. Recent Advances of Aqueous Rechargeable Zinc-Iodine Batteries: Challenges, Solutions, and Prospects. *Adv. Mater.* **2022**, *34*, 2108856.
(16) Liu, T.; Lei, C.; Wang, H.; Xu, C.; Ma, W.; He, X.; Liang, X. Practical Four-Electron Zinc-Iodine Aqueous Batteries Enabled by Orbital Hybridization Induced Adsorption-Catalysis. *Sci. Bull.* **2024**, *69*, 1674-1685.
(17) Jiang, P.; Du, Q.; Lei, C.; Xu, C.; Liu, T.; He, X.; Liang, X. Stabilized Four-Electron Aqueous Zinc-Iodine Batteries by Quaternary Ammonium Complexation. *Chem. Sci.* **2024**, *15*, 3357-3364.
(18) Zhang, P. F.; Li, J. H.; Zhang, S.; Li, D. C.; Zeng, S. Y.; Xu, S. L.; Yao, Q. X.; Liu, L. Y.; Ding, L.; Li, H. X.; et al. Toward Shuttle-Free Zn-I_2 Battery: Anchoring and Catalyzing Iodine Conversion by High-Density P-Doping Sites in Carbon Host. *Adv. Funct. Mater.* **2024**, *34*, 2306359.
(19) Li, X.; Li, N.; Huang, Z.; Chen, Z.; Liang, G.; Yang, Q.; Li, M.; Zhao, Y.; Ma, L.; Dong, B.; et al. Enhanced Redox Kinetics and Duration of Aqueous I_2/I^- Conversion Chemistry by MXene Confinement. *Adv. Mater.* **2021**, *33*, 2006897.
(20) Wang, K.; Li, H.; Xu, Z.; Liu, Y.; Ge, M.; Wang, H.; Zhang, H.; Lu, Y.; Liu, J.; Zhang, Y.; et al. An Iodine-Chemisorption Binder for High-Loading and Shuttle-Free Zn-Iodine Batteries. *Adv. Energy Mater.* **2024**, *14*, 2304110.
(21) Yang, J. L.; Liu, H. H.; Zhao, X. X.; Zhang, X. Y.; Zhang, K. Y.; Ma, M. Y.; Gu, Z. Y.; Cao, J. M.; Wu, X. L. Janus Binder Chemistry for Synchronous Enhancement of Iodine Species Adsorption and Redox Kinetics toward Sustainable Aqueous Zn-I_2 Batteries. *J. Am. Chem. Soc.* **2024**, *146*, 6628-6637.
(22) Liu, M.; Chen, Q.; Cao, X.; Tan, D.; Ma, J.; Zhang, J. Physicochemical Confinement Effect Enables High-Performing Zinc-Iodine Batteries. *J. Am. Chem. Soc.* **2022**, *144*, 21683-21691.
(23) Yang, F.; Long, J.; Yuwono, J. A.; Fei, H.; Fan, Y.; Li, P.; Zou, J.; Hao, J.; Liu, S.; Liang, G.; et al. Single Atom Catalysts for Triiodide Adsorption and Fast Conversion to Boost the Performance of Aqueous Zinc–Iodine Batteries. *Energy Environ. Sci.* **2023**, *16*, 4630-4640.
(24) Chen, Z.; Wang, F.; Ma, R.; Jiao, W.; Li, D.; Du, A.; Yan, Z.; Yin, T.; Yin, X.; Li, Q.; et al. Molecular Catalysis Enables Fast Polyiodide Conversion for Exceptionally Long-Life Zinc–Iodine Batteries. *ACS Energy Lett.* **2024**, *9*, 2858-2866.
(25) Kao, C.-C.; Liu, J.; Ye, C.; Zhang, S.; Hao, J.; Qiao, S.-Z. Building Fast and Selective Zn Ion Channels for Highly Stable Quasi-Solid-State Zn-Ion Batteries. *J. Mater. Chem. A* **2023**, *11*, 23881-23887.
(26) Yang, J. L.; Xiao, T.; Xiao, T.; Li, J.; Yu, Z.; Liu, K.; Yang, P.; Fan, H. J. Cation-Conduction Dominated Hydrogels for Durable Zinc-Iodine Batteries. *Adv. Mater.* **2024**, *36*, 2313610.
(27) Kang, Y.; Chen, G.; Hua, H.; Zhang, M.; Yang, J.; Lin, P.; Yang, H.; Lv, Z.; Wu, Q.; Zhao, J.; et al. A Janus Separator Based on Cation Exchange Resin and Fe Nanoparticles-decorated Single-wall Carbon Nanotubes with Triply Synergistic Effects for High-areal Capacity Zn-I_2 Batteries. *Angew. Chem. Int. Ed.* **2023**, *62*, e202300418.
(28) Chen, Q.; Hao, J.; Zhu, Y.; Zhang, S. J.; Zuo, P.; Zhao, X.; Jaroniec, M.; Qiao, S. Anti-Swelling Microporous Membrane for High-Capacity and Long-Life Zn-I_2 Batteries. *Angew. Chem. Int. Ed.* **2024**. DOI: 10.1002/anie.202413703.
(29) Xiao, T.; Yang, J. L.; Zhang, B.; Wu, J.; Li, J.; Mai, W.; Fan, H. J. All-Round Ionic Liquids for Shuttle-Free Zinc-Iodine Battery. *Angew. Chem. Int. Ed.* **2024**, *63*, e202318470.
(30) Zhang, S. J.; Hao, J.; Wu, H.; Chen, Q.; Ye, C.; Qiao, S. Z. Protein Interfacial Gelation toward Shuttle-Free and Dendrite-Free Zn-Iodine Batteries. *Adv. Mater.* **2024**, *36*, 2404011.
(31) Wu, H.; Hao, J.; Zhang, S.; Jiang, Y.; Zhu, Y.; Liu, J.; Davey, K.; Qiao, S. Z. Aqueous Zinc-Iodine Pouch Cells with Long Cycling Life and Low Self-Discharge. *J. Am. Chem. Soc.* **2024**, *146*, 16601–16608.
(32) Hao, J.; Yuan, L.; Zhu, Y.; Bai, X.; Ye, C.; Jiao, Y.; Qiao, S. Z. Low-Cost and Non-Flammable Eutectic Electrolytes for Advanced Zn-I_2 Batteries. *Angew. Chem. Int. Ed.* **2023**, *62*, e202310284.
(33) Zhang, P.-F.; Wu, Z.; Zhang, S.; Liu, L.-Y.; Tian, Y.; Dou, Y.; Lin, Z.; Zhang, S. Tannin Acid Induced Anticorrosive Film Toward Stable Zn-Ion Batteries. *Nano Energy* **2022**, *102*, 107721.
(34) Yang, H.; Qiao, Y.; Chang, Z.; Deng, H.; He, P.; Zhou, H. A Metal-Organic Framework as a Multifunctional Ionic Sieve Membrane for Long-life Aqueous Zinc-Iodide Batteries. *Adv. Mater.* **2020**, *32*, 2004240.
(35) Philbrick, F. A. The Hydrolysis of Iodine Monochloride. *J. Am. Chem. Soc.* **1934**, *56*, 1257–1259.
(36) Han, W.; Li, X. Electrode and electrolyte additive synergy effect for improving the capacity and supporting a high voltage plateau of aqueous rechargeable zinc iodine batteries. *J. Power Sources* **2023**, *580*, 233296.
(37) Liu, T.; Lei, C.; Wang, H.; Li, J.; Jiang, P.; He, X.; Liang, X. Aqueous Electrolyte With Weak Hydrogen Bonds for Four-Electron Zinc-Iodine Battery Operates in a Wide Temperature Range. *Adv. Mater.* **2024**, *36*, e2405473.
(38) Li, W.; Xu, H.; Zhang, H.; Wei, F.; Zhang, T.; Wu, Y.; Huang, L.; Fu, J.; Jing, C.; Cheng, J.; et al. Designing Ternary Hydrated Eutectic Electrolyte Capable of Four-Electron Conversion for Advanced Zn–I_2 Full Batteries. *Energy Environ. Sci.* **2023**, *16*, 4502-4510.
(39) Yan, L.; Zhai, Q.; Zhang, S.; Li, Z.; Kang, Q.; Gao, X.; Jin, C.; Liu, T.; Ma, T.; Lin, Z. The Burgeoning Zinc Powder Anode for Aqueous Zinc Metal Batteries: from Electrode

Preparation to Performance Enhancement. *Adv. Energy Mater.* **2024**, *14*, 2401328.
(40) Zhang, S. J.; Hao, J.; Zhu, Y.; Li, H.; Lin, Z.; Qiao, S. Z. pH-Triggered Molecular Switch Toward Texture-Regulated Zn Anode. *Angew. Chem. Int. Ed.* **2023**, *62*, e202301570.
(41) Yu, H.; Chen, D.; Li, Q.; Yan, C.; Jiang, Z.; Zhou, L.; Wei, W.; Ma, J.; Ji, X.; Chen, Y.; et al. In Situ Construction of Anode-Molecule Interface via Lone-Pair Electrons in Trace Organic Molecules Additives to Achieve Stable Zinc Metal Anodes. *Adv. Energy Mater.* **2023**, *13* (22), 2300550.
(42) Li, Z.; Wu, X.; Yu, X.; Zhou, S.; Qiao, Y.; Zhou, H.; Sun, S. G. Long-Life Aqueous Zn-I_2 Battery Enabled by A Low-Cost Multifunctional Zeolite Membrane Separator. *Nano Lett.* **2022**, *22*, 2538-2546.
(43) Cheng, Z.; Pan, H.; Li, F.; Duan, C.; Liu, H.; Zhong, H.; Sheng, C.; Hou, G.; He, P.; Zhou, H. Achieving Long Cycle Life for All-Solid-State Rechargeable Li-I_2 Battery by a Confined Dissolution Strategy. *Nat. Commun.* **2022**, *13*, 125.
(44) Zhang, S. J.; Hao, J.; Luo, D.; Zhang, P. F.; Zhang, B.; Davey, K.; Lin, Z.; Qiao, S. Z. Dual-function electrolyte additive for highly reversible Zn anode. *Adv. Energy Mater.* **2021**, *11*, 2102010.
(45) Choe, C.; Lademann, J.; Darvin, M. E. Depth profiles of hydrogen bound water molecule types and their relation to lipid and protein interaction in the human stratum corneum in vivo. *Analyst* **2016**, *141*, 6329-6337.
(46) Liu, Z.; Zhao, H.-L.; Lang, H.-Z.; Wang, Y.; Li, Z.-L.; Men, Z.-W.; Wang, S.-H.; Sun, C.-L. Raman investigation of hydration structure of iodide and iodate*. *Chinese Phys. B* **2021**, *30*, 043301.
(47) Zhao, Q.; Yu, X.; Xue, J.; Zhang, M.; Li, Z.; Wang, J.; Yang, Y.; Zou, Y.; Qiao, Y.; Sun, S.-G. Competitive Tradeoff between Zn Deposition and Hydrogen Evolution Reaction on Zn-Metal Anode. *ACS Energy Lett.* **2024**, *9*, 4102-4110.

For Table of Contents Only

